Article:

Chen, W, Kemp, DB, Newton, RJ orcid.org/0000-0003-0144-6867 et al. (4 more authors) (2022) Major sulfur cycle perturbations in the Panthalassic Ocean across the Pliensbachian-Toarcian boundary and the Toarcian Oceanic Anoxic Event. Global and Planetary Change, 215. 103884. p. 103884. ISSN 0921-8181

https://doi.org/10.1016/j.gloplacha.2022.103884

Major sulfur cycle perturbations in the Panthalassic Ocean across the Pliensbachian-Toarcian boundary and the Toarcian Oceanic Anoxic Event

Wenhan Chen [a], David B. Kemp [a*], Robert J. Newton [b], Tianchen He [b], Chunju Huang [a], Tenichi Cho [c], Kentaro Izumi [d]

[a] *State Key Laboratory of Biogeology and Environmental Geology and Hubei Key Laboratory of Critical Zone Evolution, School of Earth Sciences, China University of Geosciences, Wuhan 430074, P.R. China*

[b] *School of Earth and Environment, University of Leeds, Leeds LS2 9JT, UK*

[c] *Graduate School of Creative Science and Engineering, Waseda University, Tokyo 169-8050, Japan*

[d] *Faculty and Graduate School of Education, Chiba University, 1-33 Yayoi-cho, Inage-ku, Chiba-shi, Chiba 263-8522, Japan*

*Corresponding author: David B. Kemp (davidkemp@cug.edu.cn)

Abstract

The early Toarcian Oceanic Anoxic Event (T-OAE, ~183 Ma) was characterized by marine deoxygenation and the burial of organic-rich sediments at numerous localities worldwide. However, the extent of marine anoxia and its impact on the sulfur cycle during the T-OAE is currently poorly understood. Here, stable sulfur isotopes of reduced metal-bound sulfur ($\delta^{34}S_{pyrite}$) and pyrite sulfur concentrations (S_{PY}) have been analyzed across the Pliensbachian-Toarcian boundary (Pl-To) and the T-

OAE from the Sakahogi and Sakuraguchi-dani sections (Japan), which were deposited in the deep and shallow Panthalassic Ocean, respectively. Our data reveal marked positive $\delta^{34}S_{pyrite}$ excursions of >10‰ across both the Pl-To and the T-OAE at Sakahogi, coincident with increases in S_{PY}, and a positive excursion of >20‰ at the onset of the T-OAE at Sakuraguchi-dani. Whilst the development of deep-water anoxic/euxinic conditions could have resulted in an enhanced burial of pyrite, and also partly contributed to the positive excursion of $\delta^{34}S_{pyrite}$, variations in $\delta^{34}S_{pyrite}$ at Sakahogi were most likely controlled by elevated export production and/or preservation. On the shallow shelf generally low and highly variable S_{PY} and the positive shift in $\delta^{34}S_{pyrite}$ were likely attributable mainly to elevated sedimentation rates, with redox playing only a minor role in controlling pyrite abundance. Our discovery of a positive $\delta^{34}S_{pyrite}$ excursion across the Pl-To at Sakahogi indicates a hitherto unrecognized perturbation to the deep-water sulfur cycle, potentially associated with increased seafloor organic matter flux and pyrite burial at this time, consistent with a transient interval of anoxia.

1. Introduction

The early Toarcian Oceanic Anoxic Event (T-OAE, ~183 Ma) (Jenkyns, 1988, 2010) was an interval of marked environmental change in the Early Jurassic. The event was characterized by the widespread accumulation of organic-rich sediments (Jenkyns, 1988), extinction (particularly for benthos) (Wignall et al., 2005; Jiang et al., 2020), an increase in seawater temperature (Bailey et al., 2003; Ruebsam et al., 2020), enhanced hydrological cycling (Izumi et al., 2018a), and increased continental weathering (Cohen, et al., 2004; Kemp et al., 2020). An abrupt negative carbon isotope excursion (NCIE) associated with the T-OAE has been recognized globally in both organic and inorganic carbon reservoirs (Hesselbo et al., 2000, 2007; Kemp et al., 2005; Izumi et al., 2012; Ikeda et al., 2018; Chen et al., 2021). This NCIE has been interpreted as a massive injection of ^{12}C-enriched carbon into the biosphere, potentially from volcanism from the Karoo-Ferrar Large Igneous Province, and possibly also via the release of thermogenic (McElwain et al., 2005; Svensen et al., 2007; Heimdal et al., 2021), and/or biogenic methane (Hesselbo et al., 2000; Kemp et al., 2005; Ruebsam et al., 2019). A similar, but smaller magnitude, NCIE has also been noted at the Pliensbachian-Toarcian boundary (Pl-To; Suan et al., 2008, 2010; Littler et al., 2010; Bodin et al., 2016), which was also associated with ecological stress and seawater warming (Harries and Little, 1999; Jiang et al., 2020; Ruebsam et al., 2020).

The carbon and sulfur cycles are intimately linked because organic carbon is essential for sulfate reduction, and there is an approximately constant ratio of organic-carbon to pyrite-sulfur burial in normal marine sediments (Berner, 1970, 1982). These coupled cycles are valuable indicators of marine redox, which directly impact marine life (e.g. Danise et al., 2015). Carbon cycle perturbations have been reported worldwide during the T-OAE, but research on the sulfur cycle and its isotopic expression across the T-OAE is limited. Because of the negligible fractionation of $\delta^{34}S$ between carbonate-associated sulfate (CAS), i.e. sulfate bound into carbonate lattices, and dissolved seawater sulfate, S-isotopes derived from CAS ($\delta^{34}S_{CAS}$) can accurately trace perturbations to the marine sulfur cycle (Burdett et al. 1989). Previous work on the T-OAE has revealed positive shifts in $\delta^{34}S_{CAS}$ from a handful of sections in the Tethyan realm, which can be attributed to the increased burial of pyrite during expanded seawater deoxygenation under generally low seawater sulfate (SO_4^{2-}) concentrations conditions (Gill et al., 2011; Newton et al., 2011). In the well-studied Yorkshire T-OAE section (UK), for instance, a $\delta^{34}S_{CAS}$ shift of ~6‰ is recorded (Newton, et al., 2011). A similar shift (~5‰) was also recognized in Dotternhausen (Germany) in belemnites (Gill et al., 2011). Away from the Northern Europe, a positive shift of ~6‰ in $\delta^{34}S_{CAS}$ was recorded from Monte Sorgenza, Italy, deposited on the northwest margin of Tethys (Gill et al., 2011). Outside of Europe, the only data thus far presented are from Tibet (Southwest Tethyan realm), where a positive $\delta^{34}S_{CAS}$ excursion of ~19‰ is recorded (Newton et al., 2011).

Pyrite is the most abundant stable metal-sulfide preserved in marine sediments. S-isotope records measured from sedimentary pyrite ($\delta^{34}S_{pyrite}$)

offer a useful complementary method to that of $\delta^{34}S_{CAS}$ for reconstructing marine sulfur cycle dynamics and redox conditions in deep time, particularly in sections that are not carbonate dominated (Strauss, 1997). Records of $\delta^{34}S_{pyrite}$ can, however, be influenced by factors unrelated to redox and that instead provide insights into the nature of (and changes to) depositional conditions (e.g. Pasquier et al., 2021; Houghton et al., 2022). Thus far, no research has been conducted on $\delta^{34}S_{pyrite}$ and S_{PY} changes across both the Pl-To and the T-OAE.

Due to watermass restriction of basins on the Northern Europe (e.g. Dickson et al., 2017), the prolonged anoxia and/or euxinia inferred from these sites during the T-OAE from numerous lines of geochemical evidence (e.g. McArthur et al., 2008; Pearce et al., 2008) is unlikely to be representative of redox conditions in the global ocean (e.g. McArthur, 2019). Mo- and Tl-isotope data suggest an overall increase in the extent of anoxic/euxinic waters during the T-OAE (Dickson et al., 2017; Them et al., 2018). Nevertheless, the true extent of anoxia and the redox conditions of areas outside of Europe are largely unknown. In particular, the response of the Panthalassic Ocean (the largest ocean to have existed) during the T-OAE is uncertain. Moreover, despite the evidence for a marked carbon cycle perturbation across the Pl-To (e.g. Hesselbo et al., 2007; Littler et al., 2010; Ikeda et al., 2018), the coeval sulfur cycle and redox response to this event are unclear. In this study, we present the first $\delta^{34}S_{pyrite}$ and S_{PY} record of the Panthalassic Ocean based on analysis of two sections (Sakuraguchi-dani and Sakahogi) deposited in widely differing water depths and analyze the marine sulfur cycle from the latest Pliensbachian to the early Toarcian.

2. Geological setting

Lower Jurassic siliciclastic sedimentary rocks of the Toyora Group crop out in the Toyora area of Yamaguchi Prefecture, southwest Japan (Fig. 1). The Nishinakayama Formation of the Toyora Group consists mainly of shallow marine silty mudstones and sandstones (Nakada and Matsuoka, 2011) and is well exposed at Sakuraguchi-dani (Izumi et al., 2020; Figs. 1C and 2A). The Pliensbachian to Toarcian age of this succession is well constrained by ammonite biostratigraphy (Hirano, 1973; Tanabe, 1991; Nakada and Matsuoka, 2011), and a >35m thick record of the early Toarcian negative carbon isotope ($\delta^{13}C$) excursion is also recorded, which chemostratigraphically constrains the succession (Izumi et al., 2012; Kemp and Izumi, 2014; Izumi et al., 2018a; Fig. 2A).

The upper Pliensbachian to lower Toarcian deep-sea sedimentary succession of the Inuyama area (Aichi and Gifu Prefectures) consists mainly of bedded cherts (Fig. 1D). The Sakahogi section of the Inuyama area was deposited in the deep Panthalassic Ocean, likely below carbonate compensation depth (Matsuda and Isozaki, 1991). The Sakahogi succession comprises green-grey bedded chert with two distinctive black bedded chert and black shale intervals, both associated with CIEs (Ikeda et al., 2018; Fig. 2B). Cyclostratigraphy (Ikeda and Hori, 2014) and radiolarian biostratigraphy (Hori, 1990) indicate that the lower interval represents the Pliensbachian-Toarcian boundary and the upper interval represents the T-OAE (Ikeda et al., 2018; see also Kemp et al., 2022; Fig. 2B).

3. Analytical methods

Pyrite sulfur from 118 samples (77 from Sakuraguchi-dani and 41 from Sakahogi) was extracted using the chromium reduction method (Canfield et al., 1986). Seventy-four of these samples (35 from Sakuraguchi-dani and 39 from Sakahogi) were analyzed for $\delta^{34}S_{pyrite}$. The bulk sample powder (1-2g) was treated with ~40 mL of 1 M reduced chromium chloride ($CrCl_2$) solution and 20 mL of 6N HCl for 4 hours in a specialized pyrite extraction line at the Cohen Laboratory (University of Leeds), and the evolved hydrogen sulfide (H_2S) was purged under a nitrogen atmosphere before being trapped as Ag_2S by bubbling through an $AgNO_3$ solution (0.1M). The weight of sulfide sulfur was acquired using stoichiometric calculations on the Ag_2S mass. For isotope analysis, ~0.4 mg Ag_2S was sealed into a tin capsule with excess V_2O_5, followed by online combustion to 1050℃ under helium flow to convert to SO_2 for isotopic determination. This work was carried out at the State Key Laboratory of Biogeology and Environmental

Geology, China University of Geosciences (Wuhan), using a Thermo Delta V Plus isotope ratio mass spectrometer coupled to a Flash elemental analyzer. Sulfur isotopes are expressed in standard delta notation (δ) as per mil (‰) deviations from Vienna Canyon Diablo Troilite (VCDT). Analytical error was ~0.1‰ (1σ) based on repeated analyses of three IAEA (International Atomic Energy Agency) standard samples: IAEA-S-1 (-0.3‰), IAEA-S-2 (+22.65‰) and IAEA-S-3 (-32.5‰).

4. Results

The $\delta^{34}S_{pyrite}$ profiles at Sakahogi and Sakuraguchi-dani show broadly similar trends and features, though with distinct differences in absolute values and the magnitude of changes (Fig. 2). At Sakahogi, a marked positive $\delta^{34}S_{pyrite}$ shift with a magnitude of 11.4‰ is observed across the T-OAE (Fig. 2B), compared to a larger excursion of 24.6‰ at Sakuraguchi-dani (not including an outlying value at ~7 m; Fig. 2A). A prominent shift with a similar magnitude (12.3‰) occurs across the Pl-To at Sakahogi (Fig. 2B). The $\delta^{34}S_{pyrite}$ shifts in both sections are coeval with the respective CIEs and increased TOC. The pre- and post-excursion baseline values at Sakahogi vary between ~-50‰ and ~-42‰, in contrast to more positive baseline values (~-28‰ to ~-21‰) at Sakuraguchi-dani. In comparison to previously published $\delta^{34}S_{CAS}$ data, the excursion magnitude we observe in $\delta^{34}S_{pyrite}$ across the T-OAE (>10‰) is larger than that observed in $\delta^{34}S_{CAS}$

(~6‰) from Europe (Figs. 3C, 3D and 3E). The excursion magnitudes at Sakuraguchi-dani and Sakahogi fall either side of the magnitude calculated from Tibet by Newton et al. (2011) (~19‰; Fig. 3F). Notwithstanding marked spatial differences in $\delta^{34}S_{CAS}$ excursion magnitudes across the T-OAE, the pre-excursion values are similar (~16‰ to ~20‰) between Europe and Tibet (Fig. 3).

At Sakahogi, S_{PY} values fluctuate through the succession and vary from ~0.01 to ~8.45%, with a mean of ~0.71% (Fig. 2B). There is a slight increase across the Pl-To and a marked rise (up to ~8.45% at 224 cm) in the T-OAE interval, coincident with pronounced shifts in $\delta^{13}C_{org}$, TOC, and $\delta^{34}S_{pyrite}$. Above this, S_{PY} drops abruptly to ~0.01% (Fig. 2B). At Sakuraguchi-dani S_{PY} values are lower and highly variable, ranging from ~0.01 to ~1.50%, with a mean of ~0.37% (Fig. 2A). Although relatively variable, a general increase to ~1.38% from the onset of the T-OAE is observable, followed by a decreasing trend up-section (Fig. 2A).

5. Discussion

Sulfide in sediments primarily forms via bacterial sulfate reduction (BSR):

$$SO_4^{2-} + 2CH_2O \rightarrow H_2S + 2\,HCO_3^- \qquad (1)$$

The sulfide generated then reacts with available highly reactive Fe (Fe_{HR}) to form pyrite (Rickard 1995). Pyrite is depleted in ^{34}S relative to sulfate, and thus a significant isotopic fractionation ($\triangle^{34}S=\delta^{34}S_{SO4}-\delta^{34}S_{pyrite}$) between the parent marine sulfate and pyrite occurs during BSR. Models of the marine sulfur cycle behavior across the Ediacaran-Cambrian and the late Hirnantian indicate that globally enhanced pyrite burial would lead to elevated $\delta^{34}S_{pyrite}$ values under low marine sulfate conditions (e.g. Fike and Grotzinger, 2008; Hammarlund et al., 2012), and such enhanced pyrite burial may have characterized the early Toarcian ocean (Newton et al., 2011). However, recent work has shown that local/regional factors can act as significant, and perhaps dominant, controls on $\delta^{34}S_{pyrite}$ in marine sediments (e.g. Fry et al., 1988; Canfield, 1991; Leavitt et al., 2013; Pasquier et al., 2017, 2021; Lang et al., 2020; Liu et al., 2021; Houghton et al., 2022). As such, the interpretation of $\delta^{34}S_{pyrite}$ records demands careful evaluation of both local and global drivers of marine sulfur cycling.

5.1 Sedimentation rates

Increased sedimentation rates can decrease the connectivity of sedimentary pore water with the overlying seawater, limiting diffusional exchange and reducing (or preventing) the resupply of seawater sulfate during BSR and pyrite formation. Higher sedimentation rates can also increase the supply of highly reactive iron to the sediment relative to organic matter and sulfate, ensuring more efficient trapping of dissolved hydrogen sulfide as solid iron sulfides (Liu et al., 2021). Both these effects result in increases in $\delta^{34}S_{pyrite}$ via more closed system behavior at higher sedimentation rates (Canfield, 1991; Pasquier et al., 2017, 2021; Liu et al., 2019; Liu et al., 2021; Houghton et al., 2022).

Because of the different water depths and relative distance from land, the two study sites experienced very different rates of sedimentation prior to the Toarcian NCIE, with higher sedimentation rates at Sakuraguchi-dani than at Sakahogi. This is consistent with more negative pre-excursion baseline values of $\delta^{34}S_{pyrite}$ at the deep water Sakahogi site (around -50‰; Fig. 2B), when compared to those at Sakuraguchi-dani on the shallow and more rapidly accumulating shelf (around -28‰; Fig. 2A).

The globally synchronous Toarcian NCIE allows direct comparison of sedimentation rates between Sakahogi and Sakuraguchi-dani during the event. At the shallower Sakuraguchi-dani site the NCIE is ~35 m thick, and it is just ~0.75 m thick at Sakahogi. The Toarcian event has been linked to increases in the hydrological cycle, weathering and terrigenous sediment supply (e.g., Cohen et al., 2004; Izumi et al., 2018a; Kemp et al., 2020), and sedimentation rates are likely to have increased at Sakuraguchi-dani during this period of environmental perturbation (see for example Izumi et al., 2018a; Kemp et al., 2019). A marked increase in sedimentation rate during the early Toarcian event is therefore the likely explanation for the larger positive excursion in $\delta^{34}S_{pyrite}$ at Sakuraguchi-dani. Evidence for a marked increase in sedimentation rate within the T-OAE at Sakuraguchi-dani occurs in the form of a lithological change from mudstone to silty mudstones with sandstone (Fig. 2A; Izumi et al., 2018a), and a coeval increase in phytoclasts (indicative of increased terrestrial delivery from rivers; see Kemp et al., 2019). Indeed, the positive excursion in $\delta^{34}S_{pyrite}$ closely corresponds with the increase in sandstone and phytoclast content at Sakuraguchi-dani, providing further evidence of a sedimentation rate control (Figs. 2A and S1). Additionally, although fluctuations of shallow-water redox conditions may have contributed to the high variability in S_{PY} at Sakuraguchi-dani (see Section 5.5 below), the overall low S_{PY} recorded in this section could have largely been a consequence of high sedimentation rates. In this case, and as noted above, porewater sulfate is more rapidly depleted due to the suppression of sulfate supply from the overlying water column (e.g. Lang et al., 2020).

$\delta^{34}S_{pyrite}$ at Sakahogi was maintained at much more negative values both prior to and during the early Toarcian event because sedimentation rates were significantly lower than those on the shelf. These low sedimentation rates in an open and quiescent environment, combined with the development of anoxic waters (Kemp et al., 2022), would have favored the open system supply of sulfate for BSR and large isotopic fractionations from seawater similar to the low $\delta^{34}S_{pyrite}$ values from modern euxinic settings like the Black Sea (Wijsman et al., 2001b; Johnston et al., 2008).

The overall comparisons between the sites are consistent with measurements of $\delta^{34}S_{pyrite}$ at sites with contrasting water depths off the New Zealand coast (Pasquier et al., 2021), and with $\delta^{34}S_{pyrite}$ measurements across cycles of glacial and interglacial sedimentation in the Mediterranean (Pasquier et al., 2017). Our findings are also consistent with results from a Pleistocene shallow-water section from Italy, which emphasizes the role of sedimentation rates associated with glacial-interglacial eustatic sea-level changes, regional climate and local tectonics in controlling sedimentary $\delta^{34}S_{pyrite}$ (Houghton et al., 2022).

5.2 Organic matter supply

Culture experiments have shown that cell-specific sulfate reduction rates (csSRR) can influence sulfur-isotope fractionation, whereby faster rates of csSRR correspond to decreased isotopic fractionation (Sim et al., 2011; Leavitt, et al., 2013). This mechanism may have come into play at Sakahogi, where sedimentation rates likely remained low throughout the studied interval. An increased delivery rate of organic matter to the seafloor could elevate csSRR rates, thus reducing isotopic fractionation and elevating $\delta^{34}S_{pyrite}$ values (e.g. Pasquier et al., 2021). In addition, the source of organic matter (marine versus terrestrial) likely plays a key role in influencing the sulfate reduction rate, because marine biomass is more bioavailable for microorganisms within marine sediments compared to more refractory terrestrial organic matter (Toth and Lerman, 1977;

Mollenhauer and Eglinton, 2007). Given the strong correlations between TOC and $\delta^{34}S_{pyrite}$ at Sakahogi (Fig. 4B), it is likely that accelerated csSRR linked to an increased supply of more bioavailable organic carbon played an important role in generating the positive excursions in $\delta^{34}S_{pyrite}$ at Sakahogi at both the Pl-To boundary (TOC vs $\delta^{34}S_{pyrite}$ $R^2 = 0.79$) and the early Toarcian NCIE (TOC vs $\delta^{34}S_{pyrite}$ $R^2 = 0.55$).

At Sakuraguchi-dani, there is no correlation between TOC and $\delta^{34}S_{pyrite}$ (R^2=0.09; Fig. 4A), indicating that organic matter supply had negligible control on the positive excursion in $\delta^{34}S_{pyrite}$ across the T-OAE. This is consistent with a greater delivery of more refractory terrestrial organic matter in this shallow nearshore setting during the T-OAE (Kemp and Izumi, 2014; Izumi et al., 2018a; Kemp et al., 2019).

5.3 Marine sulfate concentrations [SO_4^{2-}] and isotopic composition ($\delta^{34}S_{SO4}$)

Isotopic fractionation (△^{34}S) during microbial sulfate reduction is up to 70‰ in modern marine sediments through a series of intermediate reduction steps when marine sulfate replenishment is sufficient (Canfield and Raiswell, 1999). However, empirical work from 81 modern aqueous systems indicates that such isotopic fractionation would decrease significantly when seawater [SO_4^{2-}] is below 5 mM (Algeo et al., 2015). Experimental data from microbial cultures suggest that the isotopic fractionation will decrease proportionally with the concentration of seawater sulfate when $[SO_4^{2-}]$ is <2 mM, and will be <10‰ when $[SO_4^{2-}]$ is <0.2 mM (Canfield, 2001; Habicht et al., 2002, 2005). Thus, a small oceanic sulfate reservoir could be an important driver for decreases in isotopic fractionation ($\triangle^{34}S$) and elevated $\delta^{34}S_{pyrite}$.

Modelling of the Toarcian $\delta^{34}S_{CAS}$ record indicates that seawater $[SO_4^{2-}]$ may have been 0.6–8 mM at this time (Gill et al., 2011; Newton et al., 2011; Han et al., 2022), suggesting that this has the potential to be a driver for changes in $\delta^{34}S_{pyrite}$. The maximum $\delta^{34}S_{pyrite}$ at Sakahogi is around -35‰. When compared to the minimum possible contemporaneous CAS value of +24‰ (Newton et al., 2011) this means that there is a minimum isotopic fractionation ($\triangle^{34}S$) of 59‰, which is inconsistent with sulfate limitation being the main driver of change in $\delta^{34}S_{pyrite}$. Thus, the different $\delta^{34}S_{pyrite}$ excursion magnitudes between Sakahogi and Sakuraguchi-dani suggest that the effect of a smaller sulfate reservoir was limited, perhaps only being discernable in the small drift to more positive values in the $\delta^{34}S_{pyrite}$ baseline for both sections.

During the T-OAE, CAS isotope records show that there was a large change to more positive $\delta^{34}S_{SO4}$ of between approximately 6 and 20‰, depending on the location (Gill et al., 2011; Newton et al., 2011; Fig. 3). This ostensibly has the potential to influence the $\delta^{34}S_{pyrite}$ record. However, two features of our $\delta^{34}S_{pyrite}$ data suggest that this had little or no influence:

Firstly, elevated $\delta^{34}S_{SO4}$ continued until the end of the Toarcian after the NCIE, whereas the positive $\delta^{34}S_{pyrite}$ excursions we observe ended within the NCIE (Fig. 3). Secondly, there is no apparent excursion in $\delta^{34}S_{CAS}$ across the Pliensbachian-Toarcian boundary event (Gill et al., 2011; Han et al., 2022). Hence, these two parameters seem divorced for this time interval.

5.4 Temperature

Increased seawater temperature associated with the emission of large amounts of CO_2 to the ocean-atmosphere system (e.g. Bailey et al., 2003; Suan et al., 2008; Ruebsam et al., 2020) could have influenced $\delta^{34}S_{pyrite}$ – for example by affecting rates of microbial sulfate reduction. However, it is difficult to predict *a priori* how temperature could have affected fractionation and the isotopic composition of pyrite because different sulfate-reducing populations tend to show widely differing responses to change in seawater temperature, with differing fractionation effects, also linked to organic matter type/quality (e.g. Canfield et al., 2006; Westrich and Berner, 1988). Evaluating the impact of temperature on $\delta^{34}S_{pyrite}$ in these records would require detailed investigation and may not be possible given the uncertainties. We suggest, however, that temperature changes are likely to be insignificant relative to the controls exerted by sedimentation rate and organic matter supply.

5.5 Anoxia

Distinct enrichments of redox-sensitive trace elements such as Mo and U at Sakahogi, coupled with markedly elevated TOC/P ratios, indicate the presence of euxinic conditions across the Pl-To and T-OAE at Sakahogi (Kemp et al., 2022). This is further supported by framboid size distribution data and pyrite analysis based on Mössbauer spectroscopy from the nearby Katsuyama section (Wignall et al., 2010; Sato et al., 2012; Fig. 1D). All these datasets suggest intensified anoxia developed close to the Pl-To boundary and extended through the Toarcian event (e.g., Kemp et al., 2022). At Sakuraguchi-dani, there is only limited evidence for ephemeral anoxia across the T-OAE from laminated sediments, trace elements and framboid data, and the environment likely remained predominantly oxic (Izumi et al., 2012, 2018b; Kemp and Izumi, 2014).

Pyrite formation and burial depends on supplies of sulfate, organic matter and highly reactive iron (Berner, 1982; Morse and Berner, 1995). Increased Fe_{HR} supply is likely to have played a part in elevating S_{PY} in the deep-water Sakahogi section facilitated by an anoxic reactive iron shuttle. This mechanism transports reactive iron from basin margin sediments and concentrates it in deeper waters (Wijsman et al., 2001a; Anderson and Raiswell, 2004; Lyons and Severmann, 2006). Hydrothermal activity can also deliver Fe_{HR} to support pyrite formation in the deep ocean (Poulton and Canfield, 2011). However, deposition of the bedded cherts at Inuyama was likely well away from the influence of any hydrothermal venting

(Matsuda and Isozaki, 1991), and the preservation of primary and globally representative isotopic signals such as Os-isotopes at Inuyama (e.g. Kuroda et al., 2010) further suggests limited influence of hydrothermal fluids.

The high S_{PY} and markedly elevated TOC across the T-OAE at Sakahogi (up to 8.45% and 34.2%, respectively) suggests increased organic carbon supply and/or preservation on the seafloor. This could have fueled BSR under anoxic conditions in the deep waters (Fig. S2). Paleomagnetic data suggest a low latitude depositional setting during the Toarcian event, close to the equatorial divergence zone (Shibuya and Samejima, 1986; Fujii et al., 1993; Ando et al., 2001; Fig. 1A). Here, high surface ocean productivity could have been maintained via optimum water temperatures and nutrient supply from upwelling. Cyclostratigrahic analysis of chert bed thicknesses in Inuyama across the T-OAE also suggests enhanced surface ocean primary productivity associated with orbitally controlled variations in summer monsoon intensity and nutrient supply to Panthalassa (Ikeda and Hori, 2014). Equally, previous work has speculated that TOC enrichment in the Inuyama area could have been further facilitated by a shorter export pathway owing to deposition on the mesopelagic to upper bathyal seafloor of a volcanic seamount rather than on the abyssal seafloor (Gröcke et al., 2011), though direct evidence for this is lacking. More recent analysis based on Cd/Mo and Co*Mn variations (indicative of the mechanisms of organic enrichment; see

Sweere et al., 2016 for details) at Sakahogi across the T-OAE suggests that anoxia enhanced the preservation of deep-water organic carbon at this site, so this may have been more important than productivity as a control on the high TOC content in these black cherts (Kemp et al., 2022).

At Sakuraguchi-dani, a paucity of suitable data precludes detailed insight into primary productivity variations, so the degree to which this might control sulfur cycling in this section are unclear. Nevertheless, the combined effects of high sedimentation rates, lower concentration of mainly terrestrial (i.e., refractory) organic carbon, and the generally suboxic-oxic depositional conditions (Kemp and Izumi, 2014; Kemp et al., 2019) can explain the much lower overall S_{PY} at this site. The high variability in S_{PY} during the T-OAE interval at Sakuraguchi-dani is consistent with ephemeral anoxia/euxinia inferred from the available relatively low-resolution ichnofabric index and framboidal pyrite size distribution data (Izumi et al., 2012; Izumi et al., 2018b).

In modern anoxic systems $\delta^{34}S_{pyrite}$ can be more negative than pyrite deposited in other settings, creating larger isotope fractionations ($\Delta^{34}S$ of ~60‰) than the long-term average record for the Jurassic of ~40‰ (e.g. Lyons, 1997; c.f. Wu et al., 2010). At both Sakuraguchi-dani and Sakahogi the shift during the NCIE is to more positive values suggesting that other controls were more dominant. This observation is important for efforts to model sulfur cycle behavior during anoxic events where larger isotopic fractionations ($\Delta^{34}S$) between sulfate and sulfide are used based on values from modern basins (e.g. Owens et al., 2013). The relationships between anoxia and $\delta^{34}S_{pyrite}$ seen at Sakuraguchi-dani and Sakahogi suggest that $\Delta^{34}S$ may stay the same or decrease because of the overriding effects of increased sedimentation rates and enhanced organic matter supply during warming driven anoxic events. This should be taken into account in future modelling efforts.

Conclusions

Our work presents the first pyrite sulfur isotope data across the Pl-To and T-OAE. The direct comparison of data from the same ocean but at widely differing water depths helps to emphasize the complexity and sensitivity of sedimentary environmental controls on $\delta^{34}S_{pyrite}$, and the utility of this proxy for understanding environmental change over Earth history.

Marked positive shifts in Panthalassic $\delta^{34}S_{pyrite}$ across the T-OAE were likely predominantly controlled by increased sedimentation rates on the shallow shelf of the Sakuraguchi-dani section, and by elevated organic carbon flux to the seafloor in the deep ocean Sakahogi section (possibly augmented by deep ocean anoxia). This response probably maintained or decreased the isotopic fractionation between seawater and buried pyrite contrary to the conditions imposed in many sulfur cycling modelling studies, and likely stemmed from the overriding effects of an increased hydrological cycle and increased productivity during these warming driven oceanic anoxic events.

The high sedimentation rates, increased proportion of refractory terrestrial carbon and generally more oxygenated setting at Sakuraguchi-dani resulted in low pyrite concentrations overall and only muted enhancement during the T-OAE interval. At Sakahogi, pyrite concentrations were massively elevated during the T-OAE from low background values due to a combination of enhanced ocean surface productivity and/or favorable preservation conditions for organic carbon, and a lack of dilution from siliciclastic material. This represents a big increase in the pyrite flux of sulfur to deep waters at this site during the T-OAE.

Our data are the first to demonstrate a $\delta^{34}S$ perturbation across the Pl-To boundary present in the deep water Sakahogi section, which points to a period of elevated seafloor organic matter flux and high pyrite burial at this time, coincident with a transient interval of anoxia. Overall, our work emphasizes that $\delta^{34}S_{pyrite}$ responds mostly to regional rather than global drivers in shallow and deep settings.

Acknowledgements

We are grateful to Yijun Xiong for the pyrite extraction at the Cohen

Laboratory, University of Leeds. We thank Zihu Zhang for $\delta^{34}S_{pyrite}$ analyses at the State Key Laboratory of Biogeology and Environmental Geology, China University of Geosciences (Wuhan). This work was supported by the National Natural Science Foundation of China (Grant No. 41888101 and No. 41772029), and the National Recruitment Program for Young Professionals (P.R. China) to DBK. RJN and TH were supported by grant NE/N018559/1 from the Natural Environment Research Council. This manuscript is a contribution to the Integrated Understanding of the Early Jurassic Earth System and Timescale (JET) ICDP project and IGCP 739.

Appendix A. Supplementary material

Supplementary material related to this article can be found on-line at https://

References

Algeo, T.J., Luo, G., Song, H., Lyons, T.W., Canfield, D.E., 2015. Reconstruction of secular variation in seawater sulfate concentrations. Biogeosciences 12, 2131–2151.

Anderson, T.F., Raiswell, R., 2004. Sources and mechanisms for the enrichment of highly reactive iron in euxinic Black Sea sediments. Am. J. Sci. 304, 203–233.

Ando, A., Kodama, K., Kojima, S., 2001. Low-latitude and Southern

Hemisphere origin of Anisian (Triassic) bedded chert in the Inuyama area, Mino terrene, Central Japan. J. Geophys. Res. 106, 1973–1986.

Bailey, T.R., Rosenthal, Y., McArthur, J.M., van de Schootbrugge, B., Thirlwall, M.F., 2003. Paleoceanographic changes of the Late Pliensbachian–Early Toarcian interval: a possible link to the genesis of an Oceanic Anoxic Event. Earth Planet. Sci. Lett. 212 (3–4), 307–320.

Berner, R.A., 1970. Sedimentary pyrite formation. Am. J. Sci. 268, 1–23.

Berner, R.A., 1982. Burial of organic carbon and pyrite sulfur in the modern ocean: its geochemical and environmental significance. Am. J. Sci. 282 (4), 451–473.

Bodin, S., Krencker, F.N., Kothe, T., Hoffmann, R., Mattioli, E., Heimhofer, U., Kabiri, L., 2016. Perturbation of the carbon cycle during the late Pliensbachian–early Toarcian: New insight from high-resolution carbon isotope records in Morocco. J. Afr. Earth Sci. 116, 89–104.

Burdett, J.W., Arthur, M.A., Richardson, M., 1989. A Neogene seawater sulfate isotope age curve from calcareous pelagic microfossils. Earth Planet. Sci. Lett. 94, 189–198.

Canfield, D.E., Raiswell, R., Westrich, J.T., Reaves, C.M., Berner, R.A., 1986. The use of chromium reduction in the analysis of reduced inorganic sulfur in sediments and shales. Chem. Geol. 54, 149–155.

Canfield, D.E., 1991. Sulfate reduction in deep-sea sediments. Am. J. Sci. 291, 177–188.

Canfield, D.E., Raiswell, R., 1999. The evolution of the sulfur cycle. Am. J. Sci. 299, 697–723.

Canfield, D.E., 2001. Biogeochemistry of sulfur isotopes. Rev. Mineral. Geochem. 43, 607–636.

Canfield, D.E., Olesen, C.A., Cox, R.P., 2006. Temperature and its control of isotope fractionation by a sulfate-reducing bacterium. Geochim. Cosmochim. Acta 70, 548–561.

Chen, W., Kemp, D.B., He, T., Huang, C., Jin, S., Xiong, Y., Newton, R.J., 2021. First record of the early Toarcian oceanic anoxic event in the Hebrides Basin (UK) and implications for redox and weathering changes. Glob. Planet. Chang. 207, 103685.

Cohen, A.S., Coe, A.L., Harding, S.M., Schwark, L., 2004. Osmium isotope evidence for the regulation of atmospheric CO_2 by continental weathering. Geology 32 (2), 157–160.

Danise, S., Twitchett, R.J., Little, C.T.S., 2015. Environmental controls on Jurassic marine ecosystems during global warming. Geology 43 (3), 263–266.

Dickson, A.J., Gill, B.C., Ruhl, M., Jenkyns, H.C., Porcelli, D., Idiz, E., Lyons, T.W., van den Boorn, S.H., 2017. Molybdenum-isotope chemostratigraphy and paleoceanography of the Toarcian Oceanic

Anoxic Event (Early Jurassic). Paleoceanography 32 (8), 813–829.

Fike, D.A., Grotzinger, J.P., 2008. A paired sulfate–pyrite δ34S approach to understanding the evolution of the Ediacaran–Cambrian sulfur cycle. Geochim. Cosmochim. Acta 72, 2636–2648.

Fry, B., Ruf, W., Gest, H., Hayes, J.M., 1988. Sulfur isotope effects associated with oxidation of sulfide by O_2 in aqueous solution. Chem. Geol. 73, 205–210.

Fujii, J., Hattori, I., Nakajima, T., 1993. A study of radiolarian biostratigraphy and magnetostratigraphy of early Mesozoic red bedded chert, central Japan. News of Osaka Micropaleontologists 9, 71–89.

Gill, B.C., Lyons, T.W., Jenkyns, H.C., 2011. A global perturbation to the sulfur cycle during the Toarcian Oceanic Anoxic Event. Earth Planet. Sci. Lett. 321 (3–4), 484–496.

Golonka, J., 2007. Late Triassic and Early Jurassic palaeogeography of the world. Palaeogeogr. Palaeoclimatol. Palaeoecol. 244, 297–307.

Gröcke, D.R., Hori, R.S., Trabucho-Alexandre, J., Kemp, D.B., Schwark, L., 2011. An open ocean record of the Toarcian oceanic anoxic event. Solid Earth 2, 245–257.

Habicht, K.S., Gade, M., Thamdrup, B., Berg, P., Canfield, D.E., 2002. Calibration of sulfate levels in the Archean Ocean. Science 298, 2372–2374.

Habicht, K.S., Salling, L., Thamdrup, B., Canfield, D.E., 2005. Effect of low sulfate concentrations on lactate oxidation and isotope fractionation during sulfate reduction by *Archaeoglobus fulgidus* strain Z. Applied and Environmental Microbiology 71, 3770–3777.

Hammarlund, E.U., Dahl, T.W., Harper, D.A.T., Bond, D.P.G., Nielsen, A.T., Bjerrum, C.J., Schovsbo, N.H., Schönlaub, H.P., Zalasiewicz, J.A., Canfield, D.E., 2012. A sulfidic driver for the end-Ordovician mass extinction. Earth Planet. Sci. Lett. 331–332, 128–139.

Han, Z., Hu, X., He, T., Newton, R.J., Jenkyns, H.C., Jamieson, R.A., Franceschi, M., 2022. Early Jurassic long-term oceanic sulfur-cycle perturbations in the Tibetan Himalaya. Earth Planet. Sci. Lett. 578, 117261.

Harries, P.J., Little, C.T.S., 1999. The early Toarcian (Early Jurassic) and the Cenomanian-Turonian (Late Cretaceous) mass extinctions: similarities and contrasts. Palaeogeogr. Palaeoclimatol. Palaeoecol. 154, 39–66.

Heimdal, T.H., Goddéris, Y., Jones, M.T., Svensen, H.H., 2021. Assessing the importance of thermogenic degassing from the Karoo Large Igneous Province (LIP) in driving Toarcian carbon cycle perturbations. Nat. Commun. 12, 6221.

Hesselbo, S.P., Gröcke, D.R., Jenkyns, H.C., Bjerrum, C.J., Farrimond, P., Bell, H.S.M., Green, O.R., 2000. Massive dissociation of gas hydrate during a Jurassic oceanic anoxic event. Nature 406 (6794), 392–395.

Hesselbo, S.P., Jenkyns, H.C., Duarte, L.V., Oliveira, L.C., 2007. Carbon-isotope record of the Early Jurassic (Toarcian) Oceanic Anoxic Event from fossil wood and marine carbonate (Lusitanian Basin, Portugal). Earth Planet. Sci. Lett. 253 (3–4), 455–470.

Hirano, H., 1973. Biostratigraphic study of the Jurassic Toyora Group, part 3. Trans. Proc. Palaeont. Soc. Japan, N.S. 90, 45–71.

Hori, S.R., 1990. Lower Jurassic radiolarian zones of SW Japan. Trans. Proc. Palaeont. Soc. Japan, N.S. 159, 562–586.

Houghton, J., Scarponi, D., Capraro, L., Fike, D.A., 2022. Impact of sedimentation, climate and sea level on marine sedimentary pyrite sulfur isotopes: Insights from the Valle di Manche section (Lower–Middle Pleistocene, southern Italy). Palaeogeogr. Palaeoclimatol. Palaeoecol. 585, 110730.

Ikeda, M., Hori, R.S., 2014. Effects of Karoo–Ferrar volcanism and astronomical cycles on the Toarcian Oceanic Anoxic Events (early Jurassic). Palaeogeogr. Palaeoclimatol. Palaeoecol. 410, 134–142.

Ikeda, M., Hori, R.S., Ikehara, M., Miyashita, R., Chino, M., Yamada, K., 2018. Carbon cycle dynamics linked with Karoo-Ferrar volcanism and astronomical cycles during Pliensbachian-Toarcian (Early Jurassic). Glob. Planet. Chang. 170, 163–171.

Izumi, K., Miyaji, T., Tanabe, K., 2012. Early Toarcian (Early Jurassic) oceanic anoxic event recorded in the shelf deposits in the northwestern Panthalassa: evidence from the Nishinakayama Formation in the Toyora area, west Japan. Palaeogeogr. Palaeoclimatol. Palaeoecol. 315, 100–108.

Izumi, K., Kemp, D.B., Itamiya, S., Inui, M., 2018a. Sedimentary evidence for enhanced hydrological cycling in response to rapid carbon release during the early Toarcian oceanic anoxic event. Earth Planet. Sci. Lett. 481, 162–170.

Izumi, K., Endo, K., Kemp, D.B., Inui, M., 2018b. Oceanic redox conditions through the late Pliensbachian to early Toarcian on the northwestern Panthalassa margin: Insights from pyrite and geochemical data. Palaeogeogr. Palaeoclimatol. Palaeoecol. 493, 1–10.

Izumi, K., Suzuki, K., Kemp, D.B., Lizuka, T., 2020. Paleogeographic and tectonic setting of the Lower Jurassic (Pliensbachian-Toarcian) Nishinakayama Formation, Toyora Group, SW Japan. Geological Journal 55, 862–874.

Jenkyns, H.C., 1988. The early Toarcian (Jurassic) anoxic event-stratigraphic, sedimentary, and geochemical evidence. Am. J. Sci. 288 (2), 101–151.

Jenkyns, H.C., 2010. Geochemistry of oceanic anoxic events. Geochem. Geophys. Geosyst. 11, Q03004.

Jiang, S., Song, H., Kemp, D.B., Dai, X., Liu, X., 2020. Two pulses of extinction of larger benthic foraminifera during the Pliensbachian-Toarcian and early Toarcian environmental crises. Palaeogeogr. Palaeoclimatol. Palaeoecol. 560, 109998.

Johnston, D.T., Farquhar, J., Habicht, K.S., Canfield, D.E., 2008. Sulphur isotopes and the search for life: strategies for identifying sulphur metabolisms in the rock record and beyond. Geobiology 6, 425–435.

Kemp, D.B., Coe, A.L., Cohen, A.S., Schwark, L., 2005. Astronomical pacing of methane release in the Early Jurassic period. Nature 437 (7057), 396–399.

Kemp, D.B., Izumi, K., 2014. Multiproxy geochemical analysis of a Panthalassic margin record of the early Toarcian oceanic anoxic event (Toyora area, Japan). Palaeogeogr. Palaeoclimatol. Palaeoecol. 414, 332–341.

Kemp, D.B., Baranyi, V., Izumi, K., Burgess, R.D., 2019. Organic matter variations and links to climate across the early Toarcian oceanic anoxic event (T-OAE) in Toyora area, southwest Japan. Palaeogeogr. Palaeoclimatol. Palaeoecol. 530, 90–102.

Kemp, D.B., Selby, D., Izumi, K., 2020. Direct coupling between carbon release and weathering during the Toarcian oceanic anoxic event. Geology 48, 976–980.

Kemp, D.B., Chen, W., Cho, T., Algeo, T.J., Shen, J., Ikeda, M., 2022.

Deep-ocean anoxia across the Pliensbachian-Toarcian boundary and the Toarcian Oceanic Anoxic Event in the Panthalassic Ocean. Glob. Planet. Chang. 212, 103782.

Kuroda, J., Hori, R.S., Suzuki, K., Gröcke, D.R., Ohkouchi, N., 2010. Marine osmium isotope record across the Triassic-Jurassic boundary from a Pacific pelagic site. Geology 38, 1095–1098.

Lang, X., Tang, W., Ma, H., Shen, B., 2020. Local environmental variation obscures the interpretation of pyrite sulfur isotope records. Earth Planet. Sci. Lett. 533, 116056.

Leavitt, W.D., Halevy, I., Bradley, A.S., Johnston, D.T., 2013. Influence of sulfate reduction rates on the Phanerozoic sulfur isotope record. Proc. Natl. Acad. Sci. USA 110, 11244–11249.

Littler, K., Hesselbo, S.P., Jenkyns, H.C., 2010. A carbon-isotope perturbation at the Pliensbachian–Toarcian boundary: evidence from the Lias Group, NE England. Geol. Mag. 147 (2), 181–192.

Liu, X., Fike, D.A., Li, A., Dong, J., Xu, F., Zhuang, G., Rendle-Bühring, R., Wan, S., 2019. Pyrite sulfur isotopes constrained by sedimentation rates: Evidence from sediments on the East China Sea inner shelf since the late Pleistocene. Chem. Geol. 505, 66–75.

Liu, J., Antler, G., Pellerin, A., Izon, G., Dohrmann, I., Findlay, A.J., Røy, H., Ono, S., Turchyn, A.V., Kasten, S., Jørgensen, B.B., 2021. Isotopically “heavy” pyrite in marine sediments due to high sedimentation rates and non-steady-state deposition. Geology 49 (7), 816–821.

Lyons, T.W., 1997. Sulfur isotopic trends and pathways of iron sulfide formation in upper Holocene sediments of the anoxic Black Sea. Geochim. Cosmochim. Acta 61, 3367–3382.

Lyons, T.W., Severmann, S., 2006. A critical look at iron paleoredox proxies: New insights from modern euxinic marine basins. Geochim. Cosmochim. Acta 70, 5698–5722.

Matsuda, T., Isozaki, Y., 1991. Well-documented travel history of Mesozoic pelagic chert in Japan: From remote ocean to subduction zone. Tectonics 10, 475–499.

McArthur, J.M., Algeo, T.J., van de Schootbrugge, B., Li, Q., Howarth, R.J., 2008. Basinal restriction, black shales, Re-Os dating, and the Early Toarcian (Jurassic) oceanic anoxic event. Paleoceanography 23 (4), PA4217.

McArthur, J.M., 2019. Early Toarcian black shales: A response to an oceanic anoxic event or anoxia in marginal basins? Chem. Geol. 522, 71–83.

McElwain, J.C., Wade-Murphy, J., Hesselbo, S.P., 2005. Changes in carbon dioxide during an oceanic anoxic event linked to intrusion into Gondwana coals. Nature 435 (7041), 479–482.

Mollenhauer, G., Eglinton, T.I., 2007. Diagenetic and sedimentological controls on the composition of organic matter preserved in California Borderland Basin sediments. Limnol. Oceanogr. 52 (2), 558–576.

Morse, J.W., Berner, R.A., 1995. What determines sedimentary C/S ratios? Geochim. Cosmochim. Acta 59, 1073–1077.

Nakada, K., Matsuoka, A., 2011. International correlation of the Pliensbachian/Toarcian (Lower Jurassic) ammonoid biostratigraphy of the Nishinakayama Formation in the Toyora Group, southwest Japan. Newsletters on Stratigraphy 44, 89–111.

Newton, R.J., Reeves, E.P., Kafousia, N., Wignall, P.B., Bottrell, S.H., Sha, J.-G., 2011. Low marine sulfate concentrations and the isolation of the European epicontinental sea during the Early Jurassic. Geology 39, 7–10.

Owens, J.D., Gill, B.C., Jenkyns, H.C., Bates, S.M., Severmann, S., Kuypers, M.M.M., Woodfine, R.G., Lyons, T.W., 2013. Sulfur isotopes track the global extent and dynamics of euxinia during Cretaceous Oceanic Anoxic Event 2. Proceedings of the National Academy of Sciences 110, 18407–18412.

Pasquier, V., Sansjofre, P., Rabineau, M., Revillon, S., Houghton, J., Fike, D.A., 2017. Pyrite sulfur isotopes reveal glacial−interglacial environmental changes. Proc. Natl. Acad. Sci. USA 114 (23), 5941–5945.

Pasquier, V., Bryant, R.N., Fike, D.A., Halevy, I., 2021. Strong local, not global, controls on marine pyrite sulfur isotopes. Sci. Adv. 7, eabb7403.

Pearce, C.R., Cohen, A.S., Coe, A.L., Burton, K.W., 2008. Molybdenum isotope evidence for global ocean anoxia coupled with perturbations to the carbon cycle during the early Jurassic. Geology 36 (3), 231–234.

Poulton, S.W., Canfield, D.E., 2011. Ferruginous conditions: a dominant feature of the ocean through Earth's history. Elements 7, 107–112.

Rickard D., 1995. Kinetics of FeS precipitation. Part 1: Competing reaction mechanisms. Geochim. Cosmochim. Acta 59, 4367–4379.

Ruebsam, W., Mayer, B., Schwark, L., 2019. Cryosphere carbon dynamics control early Toarcian global warming and sea level evolution. Glob. Planet. Chang. 172, 440–453.

Ruebsam, W., Reolid, M., Sabatino, N., Masetti, D., Schwark, L., 2020. Molecular paleothermometry of the early Toarcian climate perturbation. Glob. Planet. Chang. 195, 103351.

Sato, T., Isozaki, Y., Shozugawa, K., Matsuo, M., 2012. ^{57}Fe Mössbauer analysis of the Upper Triassic-Lower Jurassic deep-sea chert: Paleo-redox history across the Triassic–Jurassic boundary and the Toarcian oceanic anoxic event. Hyperfine Interactions 208, 95–98.

Scotese, C.R., 2001. Atlas of Earth History. Paleogeography, 1. PALEOMAP Project, Arlington, Tex, ISBN 0-9700020-0-9, p. 52.

Shibuya, H., Sasajima, S., 1986. Paleomagnetism of red cherts: a case study in the Inuyama area, Central Japan. J. Geophys. Res. 91, 105–116.

Sim, M.S., Bosak, T., Ono, S., 2011. Large sulfur isotope fractionation does not require disproportionation. Science 333, 74–77.

Strauss, H., 1997. The isotopic composition of sedimentary sulfur through time. Palaeogeogr. Palaeoclimatol. Palaeoecol. 132, 97–118.

Suan, G., Mattioli, E., Pittet, B., Mailliot, S., Lécuyer, C., 2008. Evidence for major environmental perturbation prior to and during the Toarcian (Early Jurassic) oceanic anoxic event from the Lusitanian Basin, Portugal. Paleoceanography 23 (1), PA1202.

Suan, G., Mattioli, E., Pittet, B., Lécuyer, C., Sucheras-Marx, B., Duarte, L.V., Philippe, M., Reggiani, L., Martineau, F., 2010. Secular environmental precursors to Early Toarcian (Jurassic) extreme climate changes. Earth Planet. Sci. Lett. 290 (3–4), 448–458.

Svensen, H., Planke, S., Chevallier, L., Malthe-Sørenssen, A., Corfu, F., Jamtveit, B., 2007. Hydrothermal venting of greenhouse gases triggering Early Jurassic global warming. Earth Planet. Sci. Lett. 256 (3–4), 554–566.

Sweere, T., van den Boorn, S., Dickson, A.J., Reichart, G.J., 2016. Definition of new trace-metal proxies for the controls on organic matter enrichment in marine sediments based on Mn, Co, Mo and Cd concentrations. Chemical Geology 441, 235–245.

Tanabe, K., 1991. Early Jurassic macrofauna of the oxygen-depleted epicontinental marine basin in the Toyora area, west Japan. Saito Ho-On Kai Special Publication 3, 147–161.

Them II, T.R., Gill, B.C., Caruthers, A.H., Gerhardt, A.M., Gröcke, D.R., Lyons, T.W., Marroquín, S.M., Nielsen, S.G., Trabucho Alexandre, J.P., Owens, J.D., 2018. Thallium isotopes reveal protracted anoxia during the Toarcian (Early Jurassic) associated with volcanism, carbon burial, and mass extinction. Proc. Natl. Acad. Sci. USA 115 (26), 6596–6601.

Toth, D.J., Lerman, A., 1977. Organic matter reactivity and sedimentation rates in the ocean. Am. J. Sci. 277 (4), 465–485.

van de Schootbrugge, B., McArthur, J.M., Bailey, T.R., Rosenthal, Y., Wright, J.D., Miller, K.G., 2005. Toarcian oceanic anoxic event: An assessment of global causes using belemnite C isotope records. Paleoceanography 20, PA3008.

Westrich, J.T., Berner, R.A., 1988. The effect of temperature on rates of sulfate reduction in marine sediments. Geomicrobiology Journal 6, 99–117.

Wignall, P.B., Newton, R.J., Little, C.T., 2005. The timing of paleoenvironmental change and cause-and-effect relationships during the Early Jurassic mass extinction in Europe. Am. J. Sci. 305 (10), 1014–1032.

Wignall, P.B., Bond, D.P., Kuwahara, K., Kakuwa, Y., Newton, R.J., Poulton, S.W., 2010. An 80 million year oceanic redox history from Permian to Jurassic pelagic sediments of the Mino-Tamba terrane, SW Japan, and the origin of four mass extinctions. Glob. Planet. Chang. 71, 109–123.

Wijsman, J.W.M., Middelburg, J.J., Heip, C.H.R., 2001a. Reactive iron in Black Sea sediments: implications for iron cycling. Marine Geology 172, 167–180.

Wijsman, J.W.M., Middelburg, J.J., Herman, P.M.J., Böttcher, M.E., Heip, C.H.R., 2001b. Sulfur and iron speciation in surface sediments along the northwestern margin of the Black Sea. Marine Chemistry 74, 261–278.

Woodfine, R.G., Jenkyns, H.C., Sarti,M., Baroncini, F., Violante, C., 2008. The response of two Tethyan carbonate platforms to the early Toarcian (Jurassic) oceanic anoxic event: environmental change and differential subsidence. Sedimentology 55, 1011–1028.

Wu, N., Farquhar, J., Strauss, H., Kim, S.T., Canfield, D.E., 2010. Evaluating the S-isotope fractionation associated with Phanerozoic pyrite burial. Geochimica et Cosmochimica Acta 74, 2053–2071.

Figures

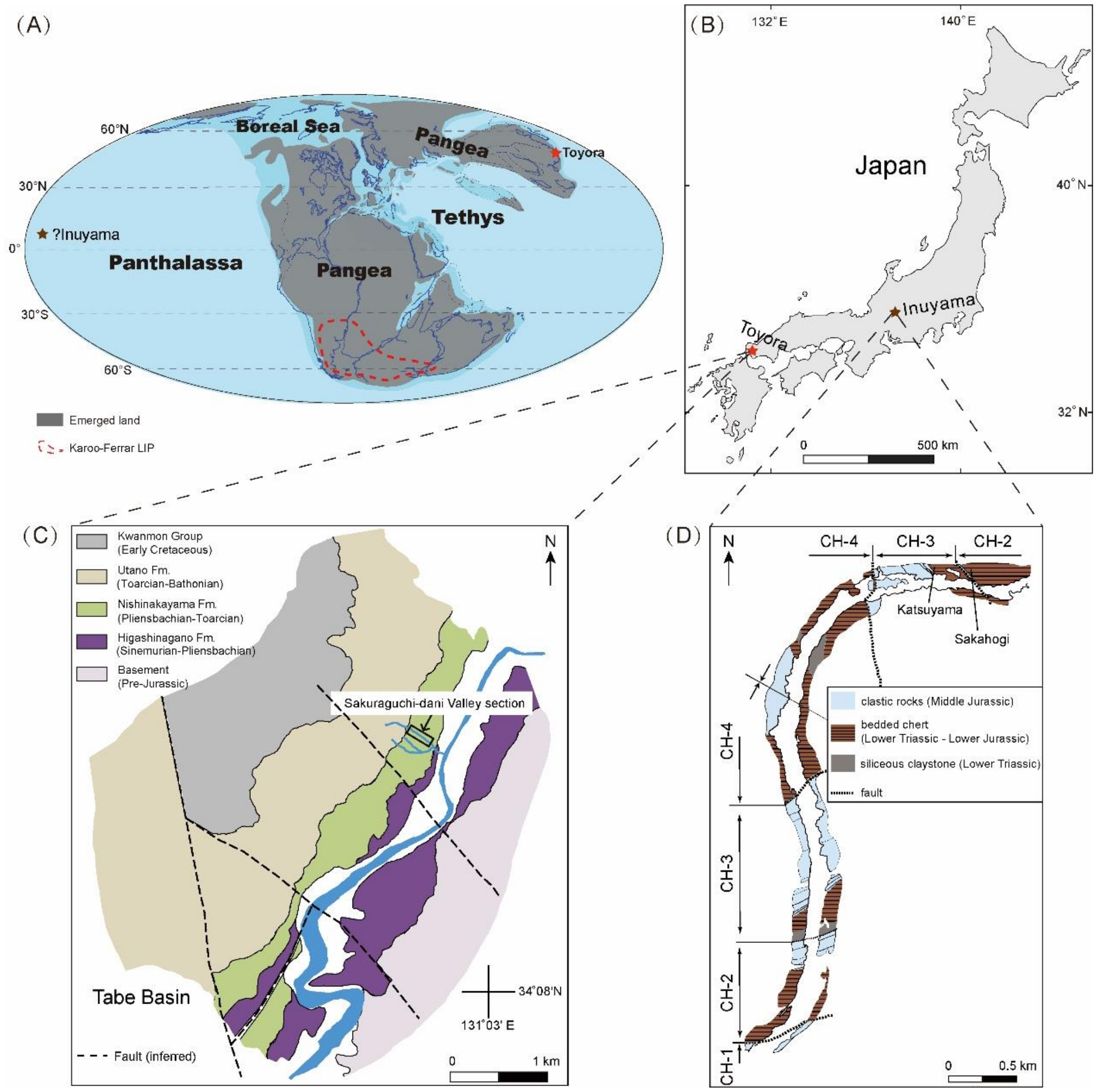

Fig. 1. (A). Paleogeographic map showing the locations of the Toyora (red star, Sakuraguchi-dani section) and Inuyama (brown star, Sakahogi section) sites in the Jurassic. Modified from Golonka (2007) and Scotese (2001). (B). Map of Japan showing the modern locations of the Toyora (red star) and Inuyama (brown star) field areas. (C). Geological map showing the Sakuraguchi-dani section in the Tabe Basin, Toyora area. Redrawn from Kemp and Izumi (2014). (D). Geologic map showing the Sakahogi

section and Katsuyama section of the Inuyama area. Redrawn from Ikeda et al. (2018).

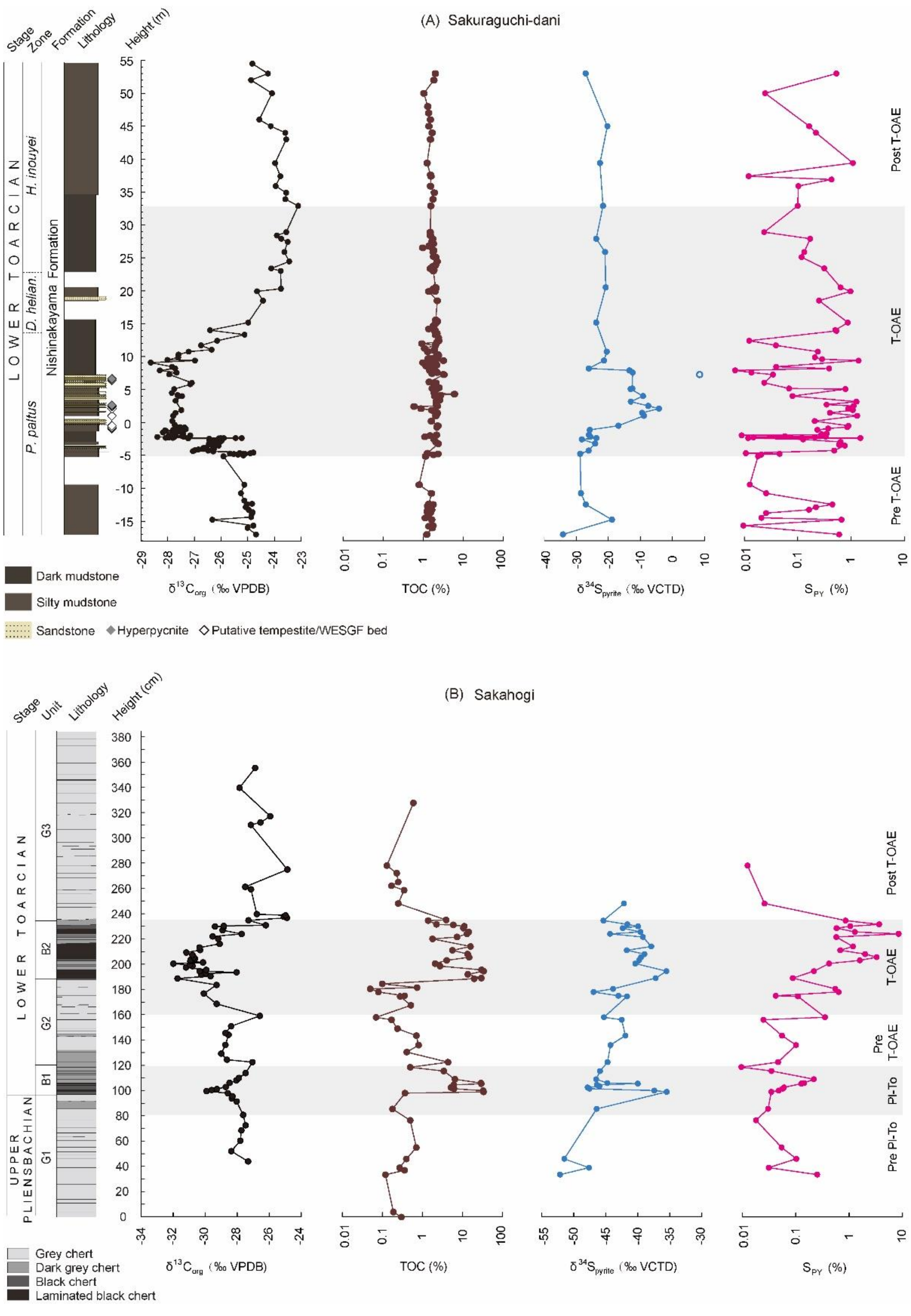

Fig. 2. Integrated organic carbon isotope ($\delta^{13}C_{org}$), total organic carbon (TOC), pyrite sulfur isotope ($\delta^{34}S_{pyrite}$), and pyrite sulfur (S_{py}) concentrations chemostratigraphy of the upper Pliensbachian-lower Toarcian at Sakuraguchi-dani (A) and Sakahogi (B), Japan. $\delta^{13}C_{org}$, TOC,

and lithostratigraphy at Sakuraguchi-dani are from Kemp and Izumi (2014) and Izumi et al. (2012, 2018a). Biostratigraphy is based on Nakada and Matsuoka (2011). $\delta^{13}C_{org}$, stratigraphic units, and lithostratigraphy at Sakahogi are from Ikeda et al. (2018) and references therein. TOC data at Sakahogi are from Kemp et al. (2022). Note that the unfilled blue circle in the Sakuraguchi-dani pyrite sulfur isotope profile represents the outlying value, and that the TOC and S_{PY} values in both sections are shown on logarithmic scales.

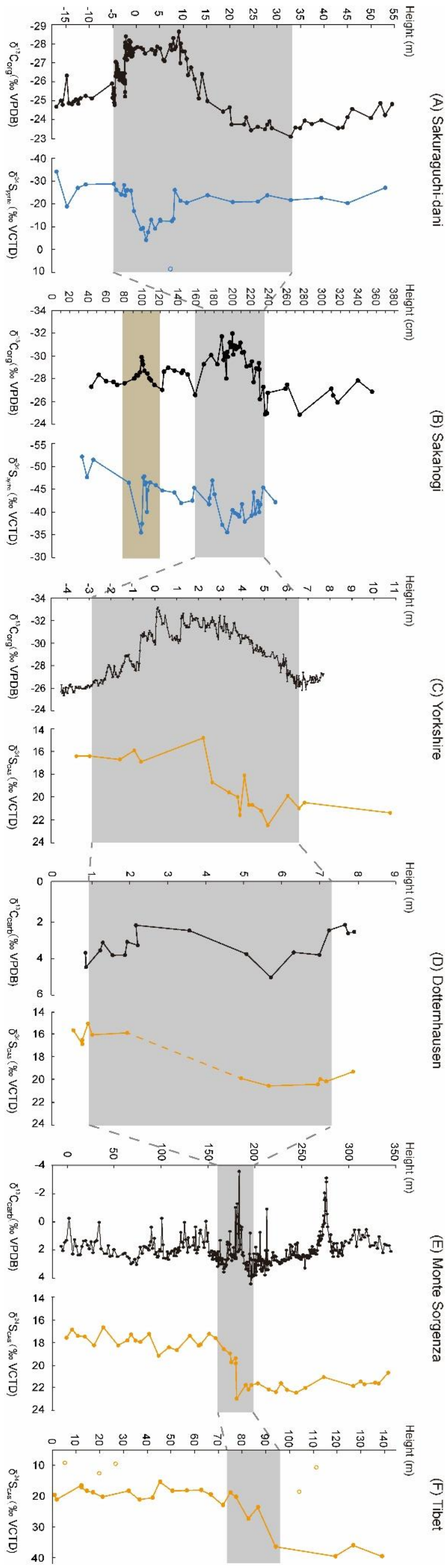
(A) Sakuraguchi-dani
Height (m)
$\delta^{13}C_{org}$ (‰ VPDB)
$\delta^{34}S_{pyrite}$ (‰ VCTD)
(B) Sakahogi
Height (cm)
$\delta^{13}C_{org}$ (‰ VPDB)
$\delta^{34}S_{pyrite}$ (‰ VCTD)
(C) Yorkshire
Height (m)
$\delta^{13}C_{org}$ (‰ VPDB)
$\delta^{34}S_{CAS}$ (‰ VCTD)
(D) Dotternhausen
Height (m)
$\delta^{13}C_{carb}$ (‰ VPDB)
$\delta^{34}S_{CAS}$ (‰ VCTD)
(E) Monte Sorgenza
Height (m)
$\delta^{13}C_{carb}$ (‰ VPDB)
$\delta^{34}S_{CAS}$ (‰ VCTD)
(F) Tibet
Height (m)
$\delta^{34}S_{CAS}$ (‰ VCTD)

Fig. 3. Excursions of $\delta^{13}C_{org}$, $\delta^{13}C_{carb}$, $\delta^{34}S_{pyrite}$, and $\delta^{34}S_{CAS}$ across the T-OAE (dark grey areas) from Sakuraguchi-dani (A), Sakahogi (B), Yorkshire (C), Dotternhausen (D), Monte Sorgenza (E) and Tibet (F). Note that $\delta^{34}S_{pyrite}$ data are shown as blue solid circles (the blue hollow circle at Sakuraguchi-dani represents an outlying value) and $\delta^{34}S_{CAS}$ data are shown as orange solid circles (the orange hollow circles at Tibet represent outlying values). The brown area at Sakahogi (B) denotes the Pl-To boundary. $\delta^{13}C_{org}$ data at Yorkshire are from Cohen et al. (2004) and Kemp et al. (2005). $\delta^{34}S_{CAS}$ data at Yorkshire are from Newton et al. (2011). $\delta^{13}C_{carb}$ and $\delta^{34}S_{CAS}$ data at Dotternhausen are from van de Schootbrugge et al. (2005) and Gill et al. (2011), respectively. $\delta^{13}C_{carb}$ and $\delta^{34}S_{CAS}$ data at Monte Sorgenza are from Woodfine et al. (2008) and Gill et al. (2011), respectively. $\delta^{34}S_{CAS}$ data at Tibet are from Newton et al. (2011).

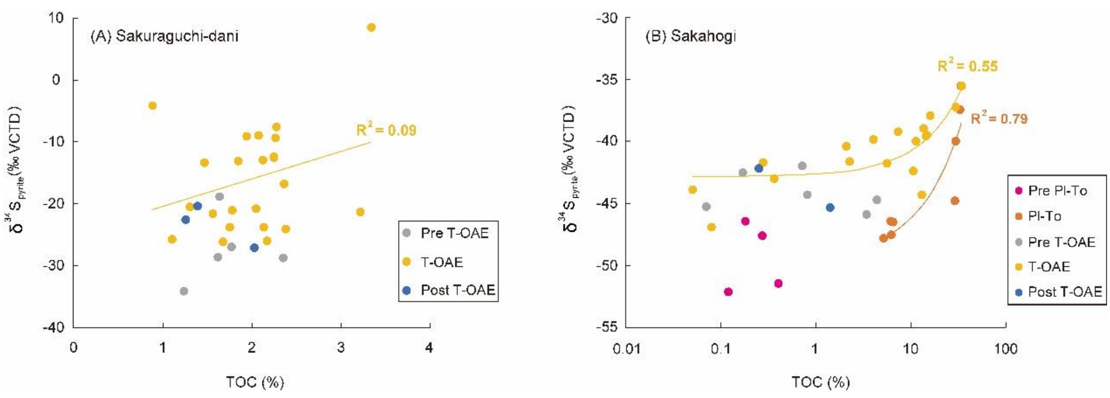

Fig. 4. Cross-plots of TOC and $\delta^{34}S_{pyrite}$ from the Sakuraguchi-dani section (A) and the Sakahogi section (B). The R^2 in each plot is the linear coefficient of determination. Note that TOC data from the Sakahogi section are shown on a logarithmic scale.